




Cite this: *RSC Adv.*, 2019, 9, 30045

A vanadate-based white light emitting luminescent material for temperature sensing

Nannan Zhang, Jie Li, Jianrong Wang, Ruixia Shi, Ling Chen,  Aiyu Zhang * and Ping Yang 

Calcium magnesium vanadate-europium vanadate powders with a homogeneous distribution have been prepared by a sol-gel method followed by a sintering process. The as-prepared powders show both broadband emission around 520 nm and sharp peak emission at 617 nm under UV light excitation, which are ascribed to the one-electron charge transfer transition in the VO_4 tetrahedra and the typical $^5\text{D}_0 \rightarrow ^7\text{F}_2$ transition of Eu^{3+} . Energy transfer occurs between the vanadate and Eu ions. The emission color of the products can be tuned by controlling the Eu concentration and temperature. White light emission can be obtained at the Eu concentration of 15% and at room temperature. The temperature related luminescence properties have been studied for the sample with 15 mol% Eu. The intensity ratio between the broadband emission (due to VO_4 tetrahedra) and the sharp peak emission (due to Eu^{3+} ions) decreases as the temperature increases in a linear relationship. The relative sensitivity (S_R) of this luminescent temperature sensor has been calculated and a maximum has been gained at 455 K with the value equal to $1.83\% \text{ K}^{-1}$.

Received 9th August 2019
Accepted 12th September 2019

DOI: 10.1039/c9ra06193b

rsc.li/rsc-advances

1. Introduction

In recent years, photoluminescent materials have attracted great interest as irreplaceable lighting devices in the area of field emission displays (FEDs), plasma display panels (PDPs), X-ray detectors, and white-light emitting diodes (w-LEDs), due to their excellent luminous efficiency and energy saving properties.^{1–5}

Among a lot of luminescent materials, rare-earth ion doped phosphors have been extensively studied and considered as potential light source materials.^{6,7} Many compounds have been applied as the matrix materials for rare-earth ions, including zinc oxides, fluorides, aluminates, silicates, zirconates, vanadates, molybdates, and phosphates.^{8–17} As an excellent red phosphor, Eu^{3+} doped YVO_4 (ref. 18 and 19) has attracted much attention from researchers, and the energy transfer from the VO_4^{3-} groups to the f-f state of Eu^{3+} ions is observed. In fact, vanadates of certain metals (Zn, Mg, Sr, Cs, K and so on) show intrinsic luminescence due to the one-electron charge transfer transition in the VO_4 tetrahedra.^{20–22}

The high-precision temperature sensing plays a key role in controlling reaction process, product performance, and safety in production.^{23–25} Physical probes such as thermometers and thermocouples, unfortunately, have limited utilities in the situation of noncontact, small volumes, as well as high spatial resolutions.^{26,27} Meanwhile, optical temperature sensors, which exploit the temperature-dependent fluorescence intensities of

thermally coupled levels (TCLs) of lanthanide ions (Ln^{3+}),^{28–36} such as Ho^{3+} , Pr^{3+} , Er^{3+} , Gd^{3+} , serves as a feasible method benefiting from the rapid-response fluorescence spectroscopy techniques. For example, Yang *et al.* proposed a strategy using optical temperature sensing behavior of Er^{3+} - Yb^{3+} co-doped $\text{NaY}(\text{MoO}_4)_2$ phosphor, and a maximum relative sensitivity value of 0.00969 K^{-1} are observed at 439 K.

In the present work, Eu^{3+} ions were introduced into a vanadate matrix $\text{Ca}_5\text{Mg}_4\text{V}_6\text{O}_{24}$ (called CMV hereafter), which show yellow-green colored luminescence emission of VO_4^{3-} under UV light excitation. Our study focused on the luminescent property and luminescent response on different temperature ranging from 300 K to 480 K.

2. Experimental section

2.1 Preparation of $\text{Ca}_5\text{Mg}_4\text{V}_6\text{O}_{24}:\text{Eu}^{3+}$ phosphors

Powders of $\text{Ca}_5\text{Mg}_4\text{V}_6\text{O}_{24}$ (CMV) with Eu^{3+} addition were prepared by a sol-gel method followed by a sintering process. 0.083 g CaCO_3 (99.99%), 0.0647 g $4\text{MgCO}_3 \cdot \text{Mg}(\text{OH})_2 \cdot 5\text{H}_2\text{O}$ (99.99%), 0.117 g NH_4VO_3 (99.9%, A.R.) and 1.051 g citric acid were mixed in a solution of HNO_3 (A.R.). The doped concentration of rare earth ion (Eu^{3+}) was from 0.5 mol% to 20 mol% (7.5×10^{-3} to 0.3 mmol) compared with the total mole amount of Ca^{2+} and Mg^{2+} in $\text{Ca}_5\text{Mg}_4\text{V}_6\text{O}_{24}$ host. The practical ratio of metal ions to citric acid that served as a chelating agent for metal ions was 1 to 2. The mixed solution was stirred under heating, dried in an oven, and finally sintered at 400°C for 3 h, then heated up to 800°C for 5 h. The obtained white powder

School of Material Science and Engineering, University of Jinan, 250022, Jinan, China.
E-mail: mse_zhangay@ujn.edu.cn; mse_yangp@ujn.edu.cn

(called CMV:Eu³⁺) was cooled down and ground for further investigation.

2.2 Preparation of luminescent device

Transparent sheets of the phosphor were prepared with Sylgard 184. Sylgard 184 (Dow Corning) is of the polydimethylsiloxane (PDMS) family and is an optically clear and inert material. About 1 g resin and 0.1 g curing agent was mixed with 0.1 g powder sample and allowed to stand at room temperature for at least 24 h. The sheet was obtained by a self-leveling method. The luminescent sheets were coated on a four-beads 310 nm LED as shown in Fig. 1. Subsequent emission observation has all been conducted to these simple devices.

2.3 Characterization

The X-ray diffraction (XRD) patterns for all target samples were registered using the Bruker D8 Advance with Cu K $\alpha_{1,2}$ radiation and 2θ range from 10° to 90°, and analyzed by using Jade-5.0 software program. The scanning electron microscope (SEM) patterns and Energy dispersive spectrometer (EDS) were obtained by using a Quanta FEG 250 Field Emission Scanning Electron Microscope. The photoluminescence (PL) and excitation (PLE) spectrum under different temperatures (above the room temperature) of the samples were evaluated with a fluorescence spectrophotometer (F-4600, Hitachi, Japan) equipped with a xenon lamp as the excitation light source. The samples sealed in a metallic box were heated to and kept at a special temperature. The measure button was pressed immediately after the sample at the special temperature being transferred from the heater into the fluorescence spectrophotometer. The temperature-related PL spectra under 0 °C were measured using a FLS920 fluorescence spectrometer with a liquid nitrogen cryostat.

3. Results and discussion

3.1 Morphology and phase distribution

In order to learn about the phase purity and crystallization of CMV:xEu³⁺ powders, the patterns of XRD were measured and

shown in Fig. 2. The pattern of CMV:xEu³⁺ ($x = 0$) matches well with 2002588 (Ca₅Mg₄V₆O₂₄) which is selected in the Crystallography Open Database (COD). With the increase of x , a new phase EuVO₄ emerges. The content of EuVO₄ phase rises dramatically with the Eu³⁺ concentration, it should be noted that the phase of EuVO₄ exists even at a concentration as low as 0.5 mol%, which indicates that EuVO₄ is easy to be formed independently rather than enter into the crystal lattice of matrix material. The products are still named as CMV:xEu³⁺ powders, although in fact they are composed of Ca₅Mg₄V₆O₂₄ and EuVO₄ phases.

A schematic of the crystal structure of Ca₅Mg₄(VO₄)₆ is presented in Fig. 3(a). In this vanadate garnet structure, Ca²⁺ ions are located in eightfold dodecahedral sites (*i.e.* a distorted cube with D_2 symmetry). The Mg²⁺ ions are in six fold octahedral sites. The metal ion V⁵⁺ (in isolated [VO₄]³⁻) completely occupies the fourfold T_d site.^{37,38} The crystal structure of Ca₅Mg₄(VO₄)₆ shows a distortion after leading 1% Eu³⁺ into the position of Ca²⁺ as shown in Fig. 3(b). The detailed data are summarized in Table 1. It is obvious that with the concentration of Eu³⁺ increasing, the lattice constant and unit cell expand modestly, and once the value of x exceeding 10%, the lattice begin to shrink slightly, indicating that the saturation of Eu³⁺ in the Ca₅Mg₄(VO₄)₆ crystalline lattice.

SEM and EDS images of CMV:xEu³⁺ ($x = 0, 15$ mol%) are presented in Fig. 4. The grain size of sample with $x = 0$ is larger than that of the one with $x = 15$ mol%. Comparing with pure CMV, the grains of CMV:15 mol% Eu³⁺ show tighter arrangement and have more unclear particle edge. According to EDS analysis, the homogeneous distribution of each elements can be found, which illustrates that the two phases CMV and EuVO₄ are combined together in the micro scale, distinguished from samples mixed mechanically.

3.2 Luminescence properties of CMV:xEu³⁺ samples

Fig. 5 exhibits PL emission and excitation spectra of typical CMV:xEu³⁺ samples. One can notice from Fig. 5(a) that the emission spectra of CMV:xEu³⁺ ($x = 1.5$ –20 mol%) consists of

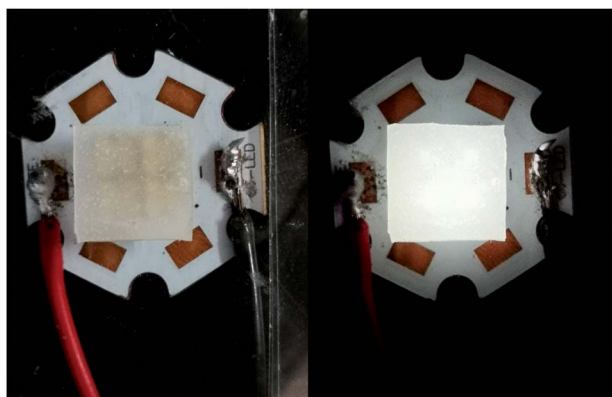


Fig. 1 Luminescent sheets on a four-beads 310 nm LED with the status of off (left) and on (right).

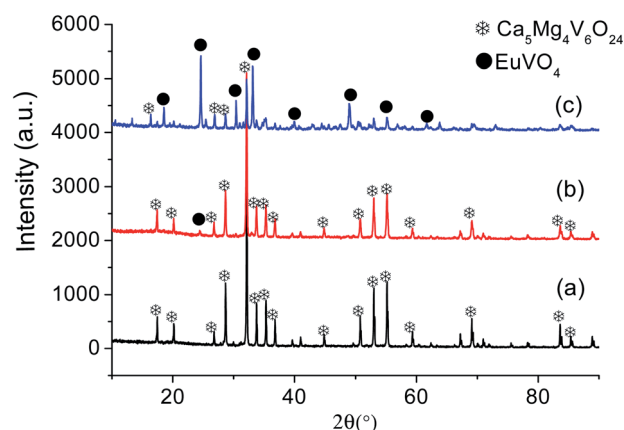


Fig. 2 XRD patterns of CMV:xEu³⁺ with $x =$ (a) 0, (b) 0.5 mol%, (c) 15 mol%.



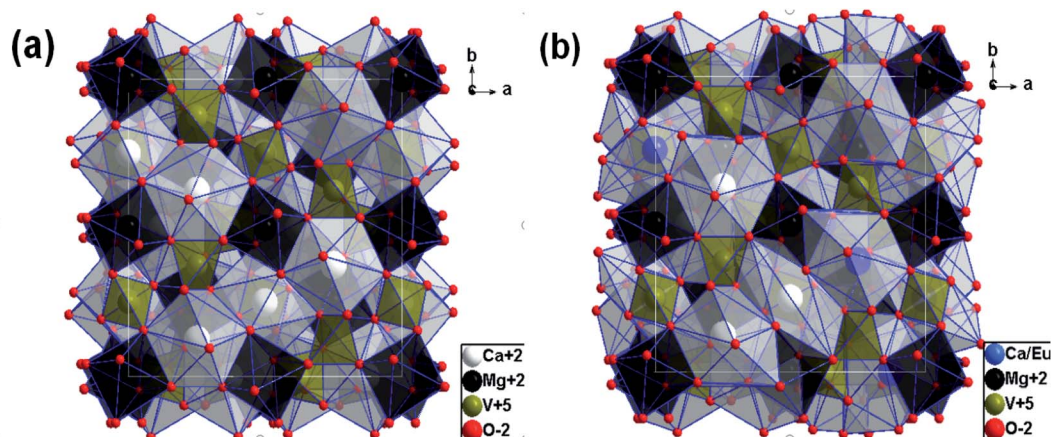


Fig. 3 Schematic view of crystal structure along *c*-direction for (a) $\text{Ca}_5\text{Mg}_4(\text{VO}_4)_6$ and (b) $\text{Ca}_5\text{Mg}_4(\text{VO}_4)_6$ with Eu^{3+} replacing 1% Ca^{2+} .

typical broadband emission and sharp peak emission while the spectrum of pure CMV only has broadband emission. The broadband emission of vanadate phosphors ranging from 400 nm to 800 nm with the maximum at 520 nm corresponds to charge transition (CT)^{7,16,17} of $[\text{VO}_4]^{3-}$. The sharp peak detected at 617 nm corresponds to electric dipole transition ($^5\text{D}_0 \rightarrow ^7\text{F}_2$) of Eu^{3+} , which indicates that Eu^{3+} ions occupy non-inversion symmetry sites in the crystal lattice. The spectra in Fig. 5(a) were normalized according to the PL intensity at 520 nm. It can be found that the relative intensity of the sharp emission peak of Eu^{3+} at 617 nm increases with the *x* value and reaches a maximum point at *x* = 15%. The relative low intensity for the sample with 20% Eu^{3+} may be attributed to concentration-quenching effect.^{39–42}

The excitation spectra of different Eu^{3+} concentration were measured at two emission wavelength, 520 nm and 617 nm, which were shown in Fig. 5(b) and (c) respectively. The excitation spectra monitored at 520 nm are typical excitation peaks of $[\text{VO}_4]^{3-}$, which show a light red-shift with Eu^{3+} concentration increasing as shown in Fig. 5(b). The excitation peak of $[\text{VO}_4]^{3-}$ is asymmetric and can be decomposed into two Gaussian components Ex_1 ($^1\text{A}_1 \rightarrow ^1\text{T}_1$, 276 nm) and Ex_2 ($^1\text{A}_1 \rightarrow ^1\text{T}_2$, 314 nm) corresponding to the intrinsic transitions in VO_4 tetrahedron^{43,44} as shown in the diagram of Fig. 6. The red-shift observed in Fig. 5(b) is actually the change of relative intensity between Ex_2 and Ex_1 , which reflects the structure modification of CMV induced by small amount of Eu^{3+} addition.

Table 1 Lattice constant and unit cell volume of CMV structure with different concentrations of Eu^{3+} (addition in the preparation process)

| <i>x</i> | <i>a</i> | <i>b</i> | <i>c</i> | α, β, γ (°) | Vol |
|----------|----------|----------|----------|-----------------------------|--------|
| 0 | 12.4630 | 12.4360 | 12.4360 | 90 | 1923.3 |
| 1.5% | 12.4397 | 12.4397 | 12.4397 | 90 | 1925.0 |
| 2.0% | 12.4399 | 12.4399 | 12.4399 | 90 | 1925.1 |
| 2.5% | 12.4453 | 12.4453 | 12.4453 | 90 | 1927.6 |
| 10% | 12.4524 | 12.4524 | 12.4524 | 90 | 1930.9 |
| 15% | 12.4461 | 12.4461 | 12.4461 | 90 | 1928.0 |
| 20% | 12.4430 | 12.4430 | 12.4430 | 90 | 1926.5 |

The excitation spectra obtained at 617 nm (Fig. 5(c)) comprise both broad band between 220 nm and 350 nm and typical sharp excitation peaks of Eu^{3+} . Both Eu – O charge

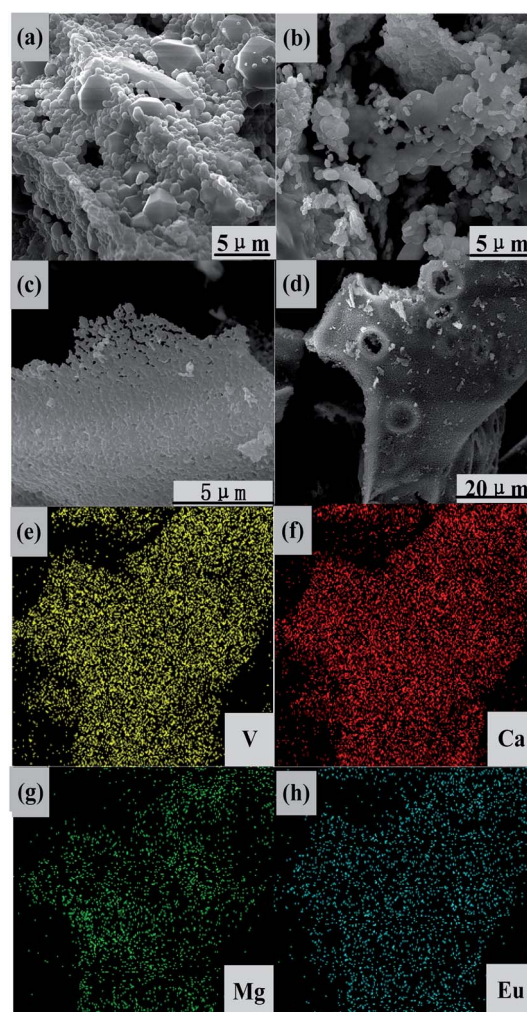


Fig. 4 SEM images of $\text{CMV}:\text{xEu}^{3+}$, (a) and (b) with *x* = 0 and (c) and (d) *x* = 15, and (e)–(h) EDS patterns based on (d).



transfer band (CTB)^{45–47} and V–O charge transfer are in the wavelength range from 220 nm to 350 nm. The broad bands in Fig. 5(c) show a blue-shift with x value which is resulted from the enhancement of the component peak around 270 nm. The excitation around 270 nm can be both ascribed to Eu–O CTB and Ex_1 of $[VO_4]^{3-}$ excitation. Based on the above discussion, we deduced that the energy of Eu^{3+} emission at 617 nm mainly come from the energy transfer between $[VO_4]^{3-}$ and Eu^{3+} at low Eu^{3+} concentration, and with the raise of Eu^{3+} concentration both energy transfer from $[VO_4]^{3-}$ to Eu^{3+} and Eu–O CTB contribute to Eu^{3+} emission at 617 nm.

No evidence of Eu^{2+} was found in all excitation and emission spectra. In addition, all the samples were prepared in air. No

reductive gas was used in the preparation process. Thus, it is convinced that all the europium element exists in the form of trivalent Eu^{3+} ions.

According to the above discussion, the emission process was illustrated by diagram in Fig. 6. After absorbing a UV photon, the electron of the tetrahedral $[VO_4]^{3-}$ group is excited from 1A_1 state to $^3T_{1,2}$ state. The energy of the excited electrons is partially transferred to Eu^{3+} ions, and emitted red light by the well-known $^5D_0 \rightarrow ^7F_J$ transitions of Eu^{3+} ions. The residual energy emitted yellow-green light by $^3T_{1,2} \rightarrow ^1A_1$ transition of $[VO_4]^{3-}$ tetrahedra.

It has been found from Fig. 5(a) that the relative intensity of 617 nm emission comparing with that of the 520 nm

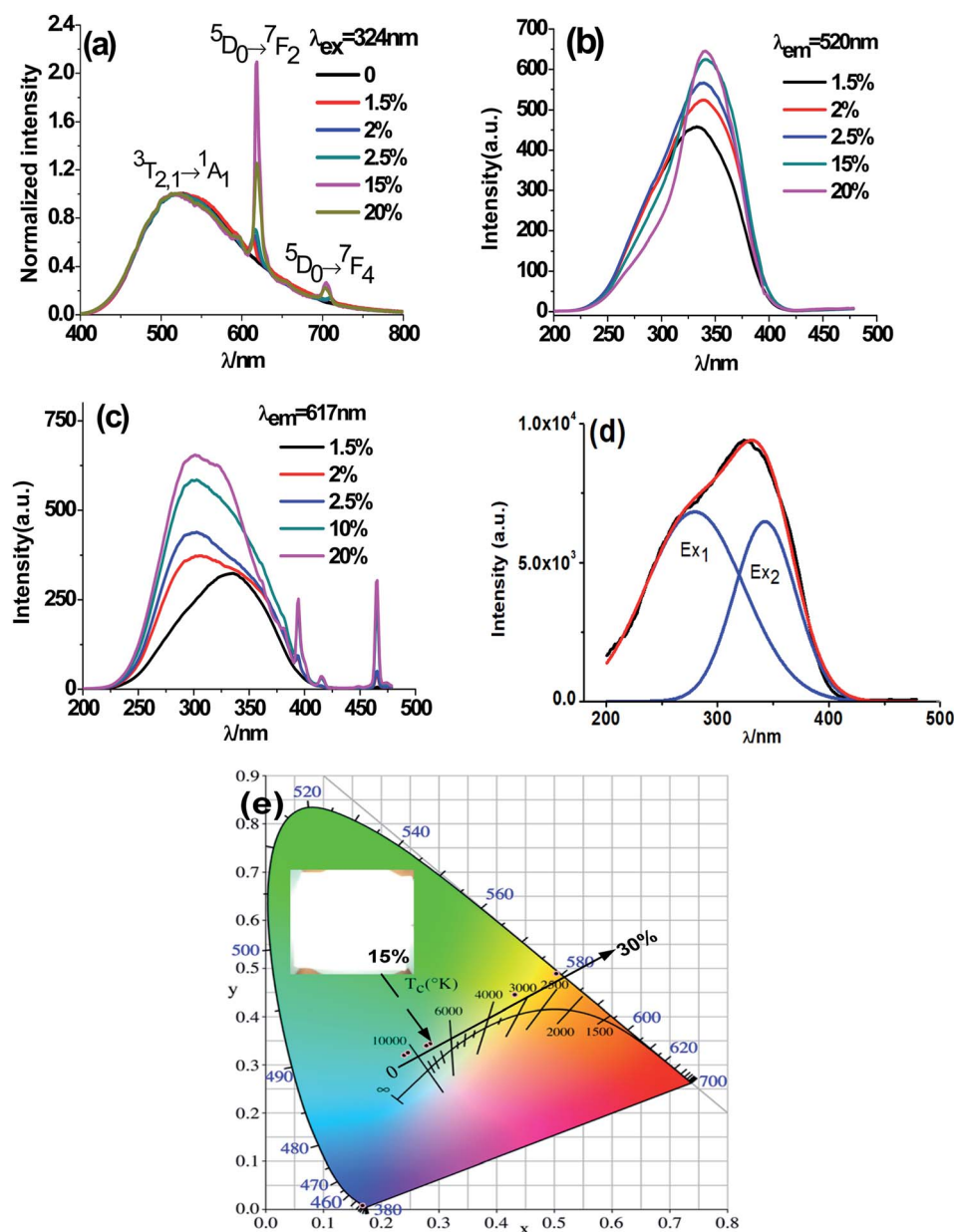


Fig. 5 (a) PL emission (normalized according to the PL intensity at 520 nm) and (b and c) excitation spectra of CMV: x mol% Eu^{3+} with different x value; (d) Gaussian peaks defined as Ex_1 and Ex_2 ; (e) CIE coordinates of samples with different Eu^{3+} concentration x ($x = 0, 10, 15, 20, 30\%$); the inset of (e), the photograph of sheet containing CMV:15 mol% Eu^{3+} under 310 nm light excitation.



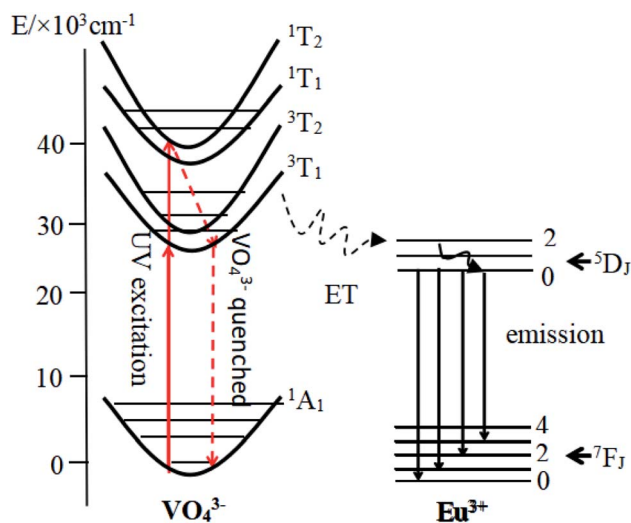


Fig. 6 The schematic diagram of energy level transition.

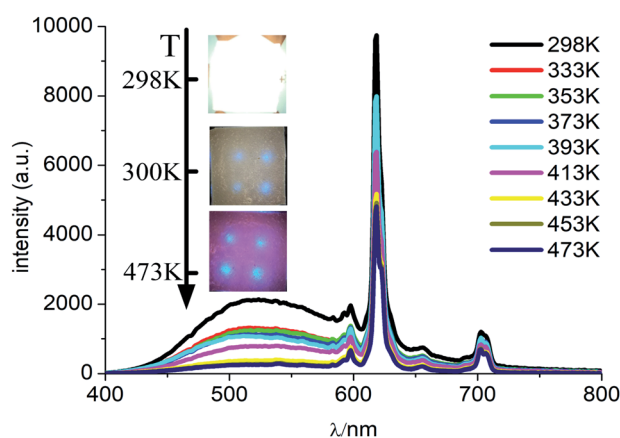


Fig. 7 PL spectra of CMV:15 mol% Eu^{3+} at different temperatures excited by 310 nm light. Inset is the photographs of the device with the UV light on at different temperature.

emission varies with Eu^{3+} concentration, so that luminous color is dependent on Eu^{3+} addition. In fact, the emission color of the obtained phosphor can be tuned easily from

yellow-green to white, and eventually to red by manipulating the addition amount of Eu^{3+} and the white light emission is gained when $x = 15\%$, which is shown in Fig. 5(e).

3.3 Temperature-dependent luminescent properties of CMV:15 mol% Eu^{3+}

In order to examine the trend of temperature-dependent luminescent properties, we carried out a study on the PL emission spectra of CMV:15 mol% Eu^{3+} powder sample at different temperature (from 300 to 480 K), which were recorded in Fig. 7.

As shown in Fig. 7, the intensities of broadband emission (at 520 nm) and sharp peak emission (at 617 nm) decrease with temperature rising, and the reducing speed at 520 nm is quicker comparing with that of 617 nm. The difference in speed could be observed in Fig. 8(a), and the ratio (defined as R) of I_{520} to I_{617} changes linearly. The luminous color is studied continuously by heating the material from 300 K to 480 K. Color changes can be observed visibly in the inset of Fig. 7, presenting that luminous color could be tuned from white to red *via* yellow. The CIE coordinates at different temperature are on a line passing by the CIE coordinate image as shown in Fig. 9. The white phosphor has a correlated color temperature of 4964 K and CIE coordinates of (0.3496, 0.3935).

Because of the temperature-dependent luminescent property, the materials may be applied as temperature sensing materials. The relative sensitivity S_R defined as the relative change of R with respect to the variation of T is obtained as follows^{20,48–50}

$$S_R = R \times \frac{dR}{dT} \quad (1)$$

where R is the ratio of I_{520} and I_{617} corresponding to different temperatures (Fig. 8(a)). T is absolute temperature. S_R value at different temperature was calculated using eqn (1) and listed in Fig. 8(b). Fitting of these data is shown as solid lines in Fig. 8(b). The calculated maximum value of S_R equals to $1.83\% \text{ K}^{-1}$ at 455 K with an excitation wavelength of 310 nm, which is a relatively high sensitivity compared

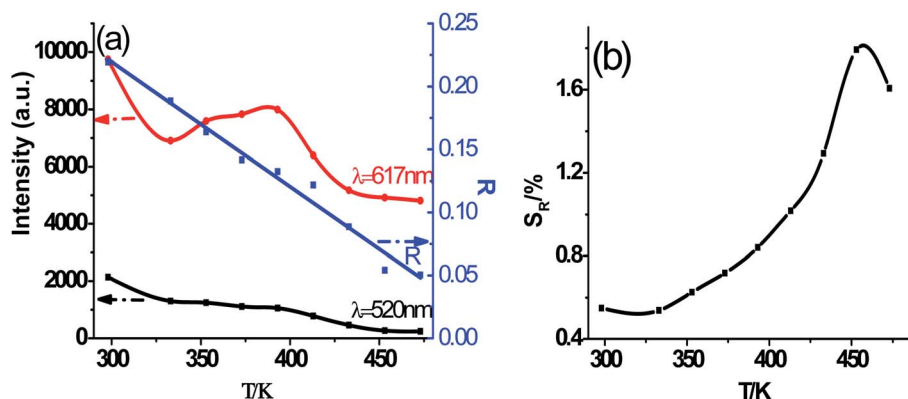


Fig. 8 (a) Luminescence intensity variation with temperature elevating at 520 nm and 617 nm, and ratio (R) of I_{520} to I_{617} , (b) the relative sensitivity (S_R).



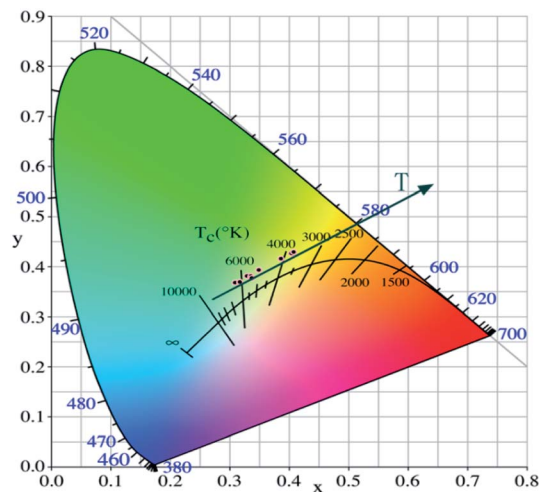


Fig. 9 CIE coordinates under different temperatures (from 300 K to 480 K).

with previously reported optical temperature sensors such as $\beta\text{-NaYF}_4\text{:Nd}^{3+}$ and $\beta\text{-NaYF}_4\text{:Yb}^{3+}/\text{Er}^{3+}$. The intrinsic yellow-green luminescence of vanadates has been reported in the previous work^{20–22}. A white-light emission can be realized in this work by introducing a common Eu^{3+} into a very low-cost $\text{Ca}_5\text{Mg}_4(\text{VO}_4)_6$ host. The obtained material shows a luminescence temperature sensing property with a high S_R . Comparing with the luminescence temperature sensor such as $\text{GdVO}_4\text{:Sm}^{3+}$ and $\text{Y}_2\text{O}_3\text{:Eu}^{3+}$ in the previous literature^{51,52}, the prepared material reaches a similar S_R in the absence of rare earth element in the host, which will result in a significant cost reduction. Interestingly, the temperature-dependent effect is limited below 293 K. The intensity ratio (R) keeps almost a constant value when the temperature is controlled under 0 °C, which is shown in Fig. 10. The mechanism of this phenomenon remains to be further studied.

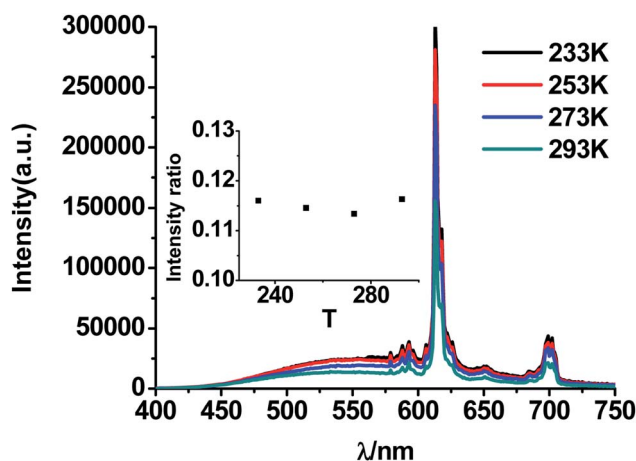


Fig. 10 PL spectra of CMV:15 mol% Eu^{3+} at different temperatures (under 0 °C) excited by 310 nm light. Inset is the ratio of I_{520} to I_{617} at different temperature (under 0 °C).

4. Conclusion

Eu -contained calcium magnesium vanadate (CMV:Eu^{3+}) phosphors were prepared and the product is a mixture of $\text{Ca}_5\text{Mg}_4\text{V}_6\text{O}_{24}$ and EuVO_4 with micro-homogeneity. The phosphor show both a broad emission with an maximum at 520 nm coordinating to CT of $[\text{VO}_4]^{3-}$ and a sharp emission around 617 nm ascribing to electric dipole transition ($^5\text{D}_0 \rightarrow ^7\text{F}_2$) of Eu^{3+} , and it can be proved that the efficient energy transfer from $[\text{VO}_4]^{3-}$ to Eu^{3+} exists. The emission color of the product can be tuned from yellow-green to red *via* white by both adjusting the Eu concentration and the temperature. The intensities of sharp emission at 617 nm first increase and then decrease with Eu^{3+} concentration, and the maximum is reached at the value of 20 mol%. The white light emission is also realized at the value of 15 mol%. The ratio between the intensities (R) of broad emission around 520 nm and that of the sharp peak at 617 nm changes linearly as the temperature rising from 295 K to 480 K. The relative sensitivity reaches the maximal value at 455 K and the maximal value equals to 1.83%, which promises a potential application of CMV:Eu^{3+} phosphor as a luminescent temperature sensor.

Conflicts of interest

There are no conflicts to declare.

Acknowledgements

This work was supported by the projects from the National Natural Science Foundation of China (grant no. 51632003, 51302106, 51501071 and 51802114).

References

- 1 K. Z. Zheng, Z. Y. Liu, C. J. Lv and W. P. Qin, *J. Mater. Chem. C*, 2013, **1**, 5502–5507.
- 2 F. C. Hawthorne, *J. Solid State Chem.*, 1977, **22**, 157–170.
- 3 G. M. Thomas and M. J. Damzen, *Opt. Express*, 2011, **19**, 4577–4582.
- 4 J. Azkargorta, M. Bettinelli, I. Iparraguirre, S. Garcia-Revilla, R. Balda and J. Fernández, *Opt. Express*, 2011, **19**, 19591–19599.
- 5 Y. J. Huang, Y. P. Huang, H. C. Liang, K. W. Su, Y. F. Chen and K. F. Huang, *Opt. Express*, 2010, **18**, 9518–9524.
- 6 M. Koichi, K. Miyamoto, S. Ujita, T. Saito, H. Ito and T. Omatsu, *Opt. Express*, 2011, **19**, 18523–18528.
- 7 Y. L. Huang, Y. M. Yu, T. Tsuboi and H. J. Seo, *Opt. Express*, 2012, **20**, 4360–4368.
- 8 D. Haranath, H. Chander, P. Sharma and S. Singh, *Appl. Phys. Lett.*, 2006, **89**, 173118.
- 9 X. Y. Liu, N. Ding, C. N. Qu, Y. S. Zhu and T. Ye, *Chin. J. Lumin.*, 2017, **38**, 587–593.
- 10 E. I. Voit, A. V. Voit, A. V. Gerasimenko and V. I. Sergienko, *J. Struct. Chem.*, 2000, **41**, 206–211.
- 11 I. A. Bondar and N. A. Toropov, *Mater. Res. Bull.*, 1967, **2**, 479–489.



- 12 A. A. Kaukis, J. E. Tiliks, V. V. Tamuzhs, A. A. Abramenskova and V. G. Vasiljev, *Fusion Eng. Des.*, 1991, **17**, 13–16.
- 13 P. R. K. Kunchala, S. N. Achary, A. K. Tyagi and B. S. Naidu, *Cryst. Growth Des.*, 2019, **19**, 3379–3388.
- 14 X. Liu, Z. Xu, C. Chen, D. Tian, L. Yang and X. Luo, *J. Mater. Chem. C*, 2019, **7**, 2361–2375.
- 15 S. E. Kichanov, Y. E. Gorshkova, G. E. Rachkovskaya, D. P. Kozlenko, G. B. Zakharevich and B. N. Savenko, *Mater. Chem. Phys.*, 2019, **237**, 121830.
- 16 J. Pejchal, J. Barta, T. Trojek, R. Kucerkova, A. Beitlerova and M. Nikl, *Radiat. Meas.*, 2019, **121**, 26–31.
- 17 C. J. Liu, Z. F. Zhou and Y. Zhang, *J. Lumin.*, 2019, **213**, 1–5.
- 18 S. M. Rafiaei, T. D. Isfahani, H. Afshari and M. Shokouhimehr, *Mater. Chem. Phys.*, 2018, **203**, 274–279.
- 19 Y. S. Chang, F. M. Huang and Y. Y. Tsai, *J. Lumin.*, 2009, **129**, 1181–1185.
- 20 X. Min, Z. Huang and M. Fang, *J. Nanosci. Nanotechnol.*, 2016, **16**, 3684–3689.
- 21 J. Y. Park, J. W. Chung and H. K. Yang, *Optik*, 2018, **155**, 384–389.
- 22 J. Huang, Q. Li and D. Chen, *Mater. Sci. Eng., B*, 2010, **172**, 108–113.
- 23 W. Xu, X. Y. Gao, L. J. Zheng, Z. G. Zhang and W. W. Cao, *Opt. Express*, 2012, **20**, 18127–18137.
- 24 V. K. Rai, D. K. Rai and S. B. Rai, *Sens. Actuators, A*, 2006, **128**, 14–17.
- 25 P. V. dos Santos, M. T. de Araujo, A. S. Gouveia-Neto, J. A. Medeiros Neto and A. S. B. Sombra, *Appl. Phys. Lett.*, 1998, **73**, 57–580.
- 26 D. G. Lee, C. R. Kesavulu, S. S. Yi, S. Cho, K. Jang, S. H. Kim and J. H. Jeong, *J. Nanosci. Nanotechnol.*, 2014, **14**, 5877–5880.
- 27 X. Min, M. H. Fang, Z. H. Huang, Y. G. Liu, C. Tang and X. W. Wu, *Inorg. Chem.*, 2014, **53**, 6060.
- 28 D. A. Hakeem and K. Park, *J. Nanosci. Nanotechnol.*, 2015, **15**, 5074.
- 29 L. K. Bharat, S. K. Jeon, K. G. Krishna and J. S. Yu, *Sci. Rep.*, 2017, **9**, 42348.
- 30 W. Xu, C. R. Li, B. S. Cao and B. Dong, *Chin. Phys. B*, 2010, **12**, 127804.
- 31 X. Yang, Z. Fu and Y. Yang, *J. Am. Chem. Soc.*, 2015, **98**, 2595–2600.
- 32 Y. M. Yang, *Ceram. Int.*, 2014, **40**, 9875–9880.
- 33 M. Quintanilla, E. Cantelar, F. Cusso and M. Villegas, *Appl. Phys. Express*, 2011, **4**, 022601.
- 34 L. Li, C. F. Guo, S. Jiang, D. K. Agrawal and T. Li, *RSC Adv.*, 2014, **4**, 6391.
- 35 P. V. dos Santos, M. T. de Araujo and J. A. Gouveia-Neto, *Appl. Phys. Lett.*, 1998, **73**, 578–580.
- 36 B. Dong, D. P. Liu, X. J. Wang, T. Yang, S. M. Miao and C. R. Li, *Appl. Phys. Lett.*, 2007, **90**, 4743.
- 37 G. Bayer, *J. Am. Ceram. Soc.*, 1965, **48**, 600.
- 38 H. Müller-Buschbaum and M. von Postel, *Z. Anorg. Allg. Chem.*, 1992, **615**, 101–103.
- 39 T. Nakajima, M. Isobe and T. Tsuchiya, *J. Phys. Chem. C*, 2010, **114**, 5160–5167.
- 40 X. Min, Z. Huang, M. Fang, Y. G. Liu, C. Tang and X. Wu, *J. Nanosci. Nanotechnol.*, 2016, **16**, 3684–3689.
- 41 J. Y. Park, J. W. Chung and H. K. Yang, *Optik*, 2018, **155**, 384–389.
- 42 Y. C. Kang and S. B. Park, *Res. Bull.*, 1999, **14**, 2611–2615.
- 43 Y. Pu, Y. Huang, T. Tsuboi, W. Huang, C. Chen and H. J. Seo, *Mater. Lett.*, 2015, **149**, 89–91.
- 44 S. Zhou, C. K. Duan and S. Han, *Dalton Trans.*, 2018, **47**, 1599–1603.
- 45 G. Blasse and B. C. Geiabmaier, *A vanadate-based white light emitting luminescent material for temperature sensing*, Springer Berlin, 1994.
- 46 G. S. Ofelt, *J. Chem. Phys.*, 1962, **37**, 511.
- 47 B. R. Judd, *Phys. Rev.*, 1962, **127**, 750.
- 48 A. F. Pereira, K. U. Kumar and W. F. Silva, *Sens. Actuators, B*, 2015, **213**, 65–71.
- 49 X. Tian, X. Wei and Y. Chen, *Opt. Express*, 2014, **22**, 30333–30345.
- 50 R. Shi, L. T. Lin and P. Dorenbos, *J. Mater. Chem. C*, 2017, **5**, 10737–10745.
- 51 J. Eldridge, *J. Lumin.*, 2019, **214**, 116535.
- 52 S. D. Li, Q. Y. Meng, S. C. Lü and W. J. Sun, *Spectrochim. Acta, Part A*, 2019, **214**, 537–543.

